

PROPERTY OF
ARGONNE NATIONAL LAB.
IDAHO LIBRARY

Argonne National Laboratory

THERMAL HYDRAULIC PERFORMANCE CHARACTERISTICS OF EBWR (0 to 100 Mwt)

by

Michael Petrick and E. A. Spleha

LEGAL NOTICE

This report was prepared as an account of Government sponsored work. Neither the United States, nor the Commission, nor any person acting on behalf of the Commission:

- A. Makes any warranty or representation, expressed or implied, with respect to the accuracy, completeness, or usefulness of the information contained in this report, or that the use of any information, apparatus, method, or process disclosed in this report may not infringe privately owned rights; or*
- B. Assumes any liabilities with respect to the use of, or for damages resulting from the use of any information, apparatus, method, or process disclosed in this report.*

As used in the above, "person acting on behalf of the Commission" includes any employee or contractor of the Commission, or employee of such contractor, to the extent that such employee or contractor of the Commission, or employee of such contractor prepares, disseminates, or provides access to, any information pursuant to his employment or contract with the Commission, or his employment with such contractor.

ARGONNE NATIONAL LABORATORY
9700 South Cass Avenue
Argonne, Illinois 60440

THERMAL HYDRAULIC PERFORMANCE
CHARACTERISTICS OF EBWR

(0 to 100 Mwt)

by

Michael Petrick and E. A. Spleha
Reactor Engineering Division

May 1963

Operated by The University of Chicago
under
Contract W-31-109-eng-38
with the
U. S. Atomic Energy Commission

TABLE OF CONTENTS

	<u>Page</u>
NOMENCLATURE	8
I. INTRODUCTION.	9
II. PARAMETERS INVESTIGATED	14
A. Volume Fraction of Steam Voids	14
B. Recirculation Flow Rate	15
C. Subcooling	15
D. "True" Liquid Level	15
E. Steam Carryunder in Downcomer	15
F. Liquid Carryover in Effluent Steam	16
III. INSTRUMENTATION.	18
A. Differential Pressure Probes	18
B. Stauschiebe Tubes	20
C. Thermocouples	26
IV. TEST PROGRAM	27
A. Preliminary	27
B. Test Series	27
V. DISCUSSION OF RESULTS.	29
A. Recirculation Flow Rates	29
B. Subcooling	32
C. Vapor Carryunder	34
D. Steam Volume Fractions in Riser and Downcomer.	37
1. Riser	38
2. Downcomer	39
E. True Liquid Level	41
F. Liquid Carryover	42
ACKNOWLEDGMENTS	44
REFERENCES.	45
APPENDIX: Tables of Data.	47

LIST OF FIGURES

<u>No.</u>	<u>Title</u>	<u>Page</u>
1.	EBWR Pressure Vessel and Internals as Designed for Operation at 20 Mwt	10
2.	Schematic of EBWR Pressure Vessel and Internals as Modified for Operation at Power Levels up to 100 Mwt	11
3.	Location of Instruments in EBWR Pressure Vessel	14
4.	Stauschiebe Tube	15
5.	Location of Liquid-carryover Sampling Probes in Steam Dome	17
6.	Schematic of Single Probe Installed Inside Pressure Vessel and Coupled with Measuring and Read-out Instrumentation. . .	19
7.	Nozzle Penetration through Upper Shielding and Pressure Vessel	21
8.	Closeup View of External Connector Head.	22
9.	Assembly of Pressure Taps to Manifold in Junction Box (cover removed) within Pressure Vessel	23
10.	Pressure Probes (P.P.) and Stauschiebe Tubes (S.T.) Installed in Pressure Vessel. Probe assembly is an integral unit which can be removed in 1 hr. Stauschiebe tubes (on vessel wall) were not removed during fueling, etc.	24
11.	Top: Thermocouple Installation in Steam Dome. Bottom: Pressure Probes Leading to Core Region and to Instrumented Fuel Subassembly (inset).	25
12.	Penetration of Instrument Leads to Terminal Boxes Mounted on Outer Surface of Biological Shielding.	25
13.	Total Recirculation Flow Rate as a Function of Reactor Power at 600 psig for Two Water Column Levels.	29
14.	Total Recirculation Flow Rate as a Function of Reactor Power at 300 psig for Two Water Column Levels.	30
15.	Comparison of Earlier with Current Total Recirculation Flow Rates at 600 psig	30
16.	Total Recirculation Flow Rate as a Function of Reactor Power at 600 psig and Various True Mixture Interface Levels	31

LIST OF FIGURES

<u>No.</u>	<u>Title</u>	<u>Page</u>
17.	Core Inlet Velocity as a Function of Reactor Power and Various True Mixture Interface Levels	31
18.	"Map" of Reactor Subcooling as a Function of Reactor Power and Various True Mixture Interface Levels.	32
19.	Measured Reactor Subcooling as a Function of Reactor Power. Increase in subcooling at 70 Mw is due to liquid carryover. Dashed curve shows subcooling predicted from measurements of liquid carryover.	33
20.	Heat Balance Flow Rates as a Function of Reactor Power . . .	34
21.	Steam Carryunder as a Function of Reactor Power and True Mixture Interface Levels	34
22.	Calculated Average Steam Volume Fraction in Core as a Function of Reactor Power.	35
23.	Comparison of Carryunder Data with the Correlation, Using Calculated Steam Volume Fraction	36
24.	Comparison of Carryunder Data with the Correlation, Using Measured Steam Volume Fraction.	36
25.	Steam Volume Fraction in Riser as a Function of Reactor Power.	37
26.	Steam Volume Fraction in Center of Riser as a Function of Reactor Power at 300 psig	37
27.	Steam Volume Fraction at Periphery of Riser as a Function of Reactor Power at 300 psig.	37
28.	Steam Volume Fraction in Center of Riser as a Function of Reactor Power at 600 psig and Various True Mixture Interface Levels.	38
29.	Steam Volume Fraction at Periphery of Riser as a Function of Reactor Power at 600 psig and Various True Mixture Interface Levels	38
30.	Effect of Subcooling on Bubble Collapse Time	40
31.	Steam Volume Fraction as a Function of Reactor Power, Showing Void Pattern Expected in Upper Region of Downcomer	41
32.	Steam Volume Fraction in Upper Region of Downcomer as a Function of Reactor Power and Various True Mixture Interface Levels.	41

LIST OF FIGURES

<u>No.</u>	<u>Title</u>	<u>Page</u>
33.	Steam Volume Fraction in Lower Region of Downcomer as a Function of Reactor Power and Various True Mixture Interface Levels.	42
34.	Height Differential between Actual Interface Level and Water Column Level as a Function of Reactor Power and Various True Mixture Interface Levels	42
35.	Percent Liquid Carryover as a Function of Reactor Power, Showing Comparison of Data Obtained from Three Sources . .	43
36.	Percent Liquid Carryover as a Function of Distance above Vapor Interface for Various Superficial Vapor Velocities . . .	43
37.	Liquid Carryover as a Function of Reactor Power and Various Water Column Levels. (Data from heat balance on Primary Reboiler)	43

LIST OF TABLES

<u>No.</u>	<u>Title</u>	<u>Page</u>
1.	Reactor Operating Conditions - Test Series No. 1	28

APPENDIX

A-1.	Summary of Reactor Data	48
A-2.	Summary of Liquid Carryover Data	49

NOMENCLATURE

c	Specific heat at constant pressure, Btu/(lb)(°F)
\bar{c}_d	Drag coefficient, dimensionless
C	Calibration constant, dimensionless
D	Diameter, ft or mm
g	Gravitational constant, ft/sec ²
G	Mass velocity, lb/(hr)(ft ²)
h	Enthalpy, Btu/lb
H	Height of the interface, ft
k	Thermal conductivity, Btu/(sec)(ft)(°F)
L	Length, ft
ΔP_A	Acceleration losses, lb/ft ²
ΔP_F	Frictional losses, lb/ft ²
ΔP_H	Head losses, lb/ft ²
ΔP_t	Total pressure drop, lb/ft ²
Δt	Time differential, sec
ΔT_{sub}	Degrees of subcooling, °F
Q	Reactor power, Btu/hr
q	Head, ft
R	Instantaneous bubble radius, ft
R_i	Bubble radius at the beginning of any time interval, ft
t	Time, sec
V	Velocity, ft/sec
W	Flow rate, lb/hr
X	Steam quality, dimensionless

Dimensionless Numbers

Pr	Prandtl number, $c\mu/k$
Fr	Froude number, V^2/gD

Greek Letters

α	Void fraction, dimensionless
μ	Dynamic viscosity, lb/(ft)(sec)
ν	Kinematic viscosity, ft ² /sec
ρ	Density, lb/ft ³
$\bar{\rho}$	Mean density, lb/ft ³
σ	Surface tension, lb/ft

Subscripts

D	Downcomer
e	Exit
ent	Gas entrainment velocity in downcomer
f	Saturation liquid
fg	Latent heat of vaporization
g	Actual gas velocity
I	Ion exchanger
IE	Intermediate heat exchanger
in	Core inlet
M	Feed water
P	Power
R	Riser
PR	Primary Reboiler
S	Steam dome
T	Total recirculation
v	Saturation vapor

THERMAL HYDRAULIC PERFORMANCE CHARACTERISTICS OF EBWR

(0 to 100 Mwt)

by

Michael Petrick and E. A. Spleha

I. INTRODUCTION

The Experimental Boiling Water Reactor (EBWR) was originally designed as a prototype reactor to produce 20 Mw of heat in the form of 600-psig steam. The original reactor system is shown in Fig. 1. The design power of 20 Mwt was readily exceeded. Moreover, after a series of extensive stability tests, the reactor with the 4-ft-diameter core attained a power level of 61.7 Mwt.

On the basis of data from these tests, a decision was made to attempt to increase the power level to 100 Mwt. A preliminary design study was carried out to estimate the probable performance characteristics and to explore some of the major problems that might be encountered during operation at 100 Mwt. The successful operation of the EBWR core at 61.7 Mwt was used as a basis for comparison. The results of this study indicated that the recirculation flow rates within the reactor would have to be increased substantially in order to minimize the steam-void fraction in the core. As a result, the modification of the EBWR internals for operation at higher power was directed primarily toward achieving this goal. The major modifications that were made are described briefly below.

Redesign of Riser - The riser was redesigned to obtain additional height and to increase its effectiveness. The additional riser height was needed to increase the recirculation flow rate and to maintain an acceptable void content within the core. The effectiveness of the original riser (basically, the control rod guide structure) was questionable. The benefit of the longer riser in the central region (where it is needed most) tended to be nullified by shorter peripheral risers due to the issuance of steam therefrom and to the cross flow of the fluid from the central portion.

The new riser arrangement (Fig. 2) is basically an extension of the original system. The desirable features of the original riser geometry are retained: control rod guidance and partial self-regulation over individual sectors of the core. The top, necked-down portion of the riser provides additional driving head and is insensitive to fluctuations of local core power. The total height of the riser is approximately 7.5 ft. This

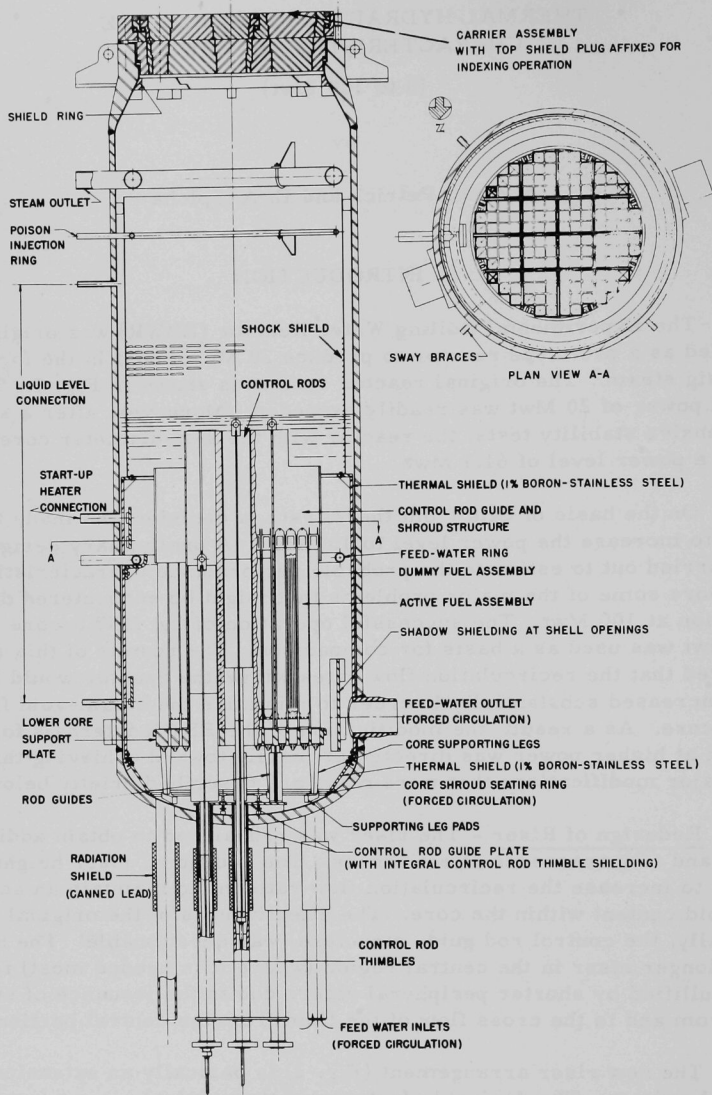


Fig. 1. EBWR Pressure Vessel and Internals as Designed for Operation at 20 Mwt

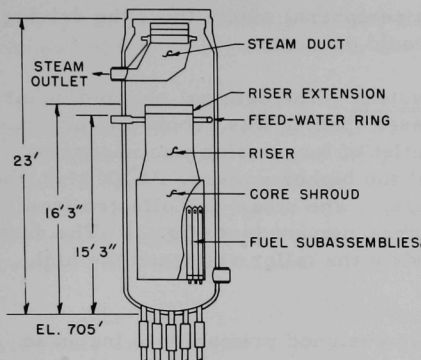


Fig. 2. Schematic of EBWR Pressure Vessel and Internals as Modified for Operation at Power Levels up to 100 Mw
112-2611

Fig. 2). The ring was designed so that jets of water emerging from it would mix with the recirculating downcomer water to effect maximum water entrainment and provide maximum downcomer coverage. Any steam carried under in the downcomer, therefore, would be mixed immediately with the cold feed water and quenching would be initiated rapidly. As a result, the maximum amount of the natural-circulation driving head available would be utilized.

The configuration of the feed-water ring considered most effective featured 72 holes (of $\frac{3}{8}$ -in. diameter) on 5° centers along the circumference, and machined at alternately 30° and 60° with respect to the horizontal plane.

A feed-water inlet nozzle of larger diameter (6 in. vs. 3 in.) was installed in the pressure vessel to allow injection of water at the desired flow rate without excessive pressure drop.

Enclosing the Core with a Cylindrical Shell and Providing a Tight Closure between Riser and Core - These modifications were intended to prevent short circuiting of the fluid from the downcomer to the peripheral riser sections and the core due to static pressure differences that are inherent in such systems. It is believed that short circuiting of the fluid may have contributed, in part, to the discrepancy between previously measured and calculated rates of coolant flow. The make-up water from the feed-water ring in the original EBWR geometry was injected at the junction of the riser and core. Short circuiting of the cold water at this point

height was chosen as the maximum feasible because of operational considerations for maintaining the steam-water interface within a desired level range and for minimizing the liquid carryover. The top portion of the riser was necked down in the hope that the increased downcomer area and resultant reduced velocity of the water would aid the de-entrainment of steam in the downcomer.

Relocation and Resizing of Feed-water Injection Ring and Inlet Nozzle - The effectiveness of the riser system was enhanced by installing a feed-water injection ring of larger diameter (4 in. vs. 2 in.) below the top of the riser (see

would collapse some of the voids in the peripheral riser; thus, the driving head and the recirculation flow rates would decrease.

Redesign of Steam-discharge System - The original steam-discharge ring was removed and the pressure vessel opening was rebored to accommodate a 10-in. discharge line. The outlet of larger size was necessary because of the increased steam loads at the higher powers. At 100 Mwt, the steam load is approximately 340,000 lb/hr. The steam is collected from the top of the reactor vessel by a duct arrangement (see Fig. 2). The duct arrangement was installed to accommodate the taller riser and the high liquid levels.

The foregoing modifications were designed primarily to increase the rates of recirculation flow in the core and to minimize the void content within the core. However, by adding the taller riser and raising the operating water level, the problem of steam-water separation became greatly aggravated. It was recognized that the probability of achieving 100 Mwt would depend, to a large degree, on solving the problem of vapor-liquid separation. The problem of steam separation can be broken down to three main parts: (1) steam carryunder in the downcomer; (2) liquid carryover in the effluent steam; and (3) vapor holdup in the two-phase mixture above the riser discharge.

The seriousness of the problem of steam carryunder is governed by the quantity of steam entrained and by the rapidity with which the entrained steam bubbles are quenched. Steam carryunder reduces the reactor subcooling which, in turn, increases the reactor void content. Steam carryunder can also reduce the natural-circulation driving head and, hence, the recirculation velocity. It was believed that in EBWR the problem of water carryover by the effluent steam would be acute because of: (1) the reduction of the volume of the steam dome effected by the taller riser; and (2) the sharp increase of the superficial steam velocity at 100 Mwt, which was expected to be approximately 1.9 ft/sec. Utilizing the meager information on natural vapor-liquid separation, it was estimated that the liquid carryover could range from 3 to 15 w/o, depending upon the location of the interface.

In a closed vessel such as EBWR, the location of the interface between the two-phase mixture and the steam dome depends upon the initial water level and upon the steam void content in the system. The voids that are formed in the reactor core and riser, and are entrained in the downcomer, displace an equal amount of water. This causes an increase in the true liquid height. The water level above the riser is further expanded by the vapor flowing through it. The final height of this two-phase mixture, therefore, is a function of the superficial steam velocity and water content above the riser. For a given initial water level at saturation (with no voids present), the expansion of the mixture increases with increasing power

because of the higher superficial steam velocity and the increased water content which is expelled from the region below the riser.

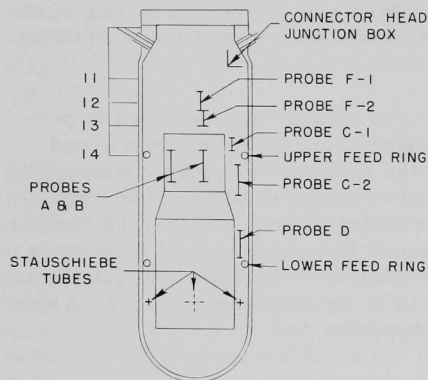
Because the degree of primary steam separation that would take place within the reactor vessel was virtually unknown and because of the tremendous effect this could have on the reactor performance characteristics, a decision was made to instrument the reactor extensively. Data on performance characteristics would afford a better understanding of the processes occurring within the reactor vessel and, also, a more realistic evaluation of EBWR-type reactors.

The instrumentation installed in the reactor was designed to provide data or information on the recirculation flow rate, volumetric and weight fraction of vapor carryunder in the downcomer, reactor subcooling, riser void fractions, quenching rate of the entrained vapor in the downcomer, location of the true two-phase mixture interface within the reactor, and liquid carryover in the effluent steam. The experimental techniques that were used, the instrumentation complex that was built to acquire these data, and the data obtained are discussed in the following sections. A complete tabulation of the data is given in Appendix A.

II. PARAMETERS INVESTIGATED

A. Volume Fraction of Steam Voids

Determination of the steam volume fraction at key positions in the reactor vessel provide data and information about a number of the problems. With reference to Fig. 3, measurements of steam volume fraction at positions



positions C-1, C-2, and D provide information on the magnitude of steam carryunder. The steam volume fraction at position C-1 is a measure of the volumetric steam carryunder rate before mixing occurs with the colder make-up water. Measurements of steam volume fraction at positions C-2 and D indicate how far the steam is entrained before complete quenching is achieved. These positions also afford some indication of the reduction of the net recirculation driving head resulting from the steam carryunder.

Fig. 3. Location of Instruments in
EBWR Pressure Vessel
112-2646

The steam volume fraction within the riser was measured at positions A and B. In addition to

serving as a basis for comparison with the calculated performance characteristics of the reactor, the data obtained were used to calculate the slip-phase velocity or velocity ratio between the steam and water.

Information on the vapor holdup above the riser discharge was obtained at positions F-1 and F-2. The data obtained were used to locate the vapor-liquid interface and, also, for comparison with the very limited laboratory data.

The steam volume fraction was derived from measurements of static differential pressure at the positions indicated. The volumetric steam fraction was computed from the relation

$$\Delta P_t = \Delta P_H + \Delta P_F + \Delta P_A \quad . \quad (1)$$

For all practical purposes, the frictional pressure drop can be neglected. The velocities, in general, are low and the equivalent diameters are large where the measurements were made. The acceleration losses, if any, are also quite small. Therefore,

$$\Delta P_t = (1 - \alpha)L\rho_f + \alpha\rho_v L = \rho_f L + \alpha(\rho_v - \rho_f)L \quad ; \quad (2)$$

$$\alpha = \frac{\Delta P_t - L\rho_f}{(\rho_v - \rho_f)L} = \frac{L\rho_f - \Delta P_t}{L(\rho_f - \rho_v)} \quad . \quad (3)$$

B. Recirculation Flow Rate

Because of the occurrence of carryunder, the recirculation flow rate can no longer be determined by the subcooling technique. An impact meter was, therefore, selected for measurement of the recirculation velocity. From the various types of impact meters available, a Stauschiebe tube (see Fig. 4) was selected because it yields an approximately 50% greater reading than the normal impact meter, such as a Pitot tube. Basically, the Stauschiebe tube is a modification of the static Pitot tube. It is less sensitive to misalignment errors, but must be calibrated. The increased reading of a Stauschiebe tube stems from the increased pressure gradient produced by the flow around a cylinder. Three Stauschiebe tubes were placed in the downcomer, approximately 120° apart, and at three radii to obtain equal area readings.

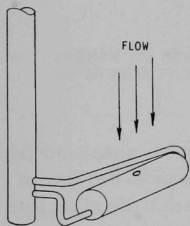


Fig. 4

Stauschiebe Tube

C. Subcooling

Subcooling measurements were made with insulated chromel-alumel thermocouples sheathed in $\frac{1}{16}$ -in.-OD tubes. Six couples were located at various positions in the downcomer on a plane approximating the bottom of the reactor core. Three couples were attached to the Stauschiebe tubes.

D. "True" Liquid Level

The vapor-liquid interface was located by a series of differential pressure readings taken from five taps penetrating the reactor vessel in the region of riser discharge (see Fig. 3, positions 11, 12, 12, and 14). Comparison of the readings with equivalent lengths of pure steam and saturated water permits the vapor-liquid interface to be pin-pointed within a limited height range.

E. Steam Carryunder in Downcomer

The steam carryunder was calculated from the measured recirculation flow rates and subcooling by means of the following heat balance:

$$\frac{W_T}{W_T - W_I} (h_f - h_{in}) - \frac{W_I}{W_T - W_I} (h_f - h_I) + X_D(h_{fg}) = X_R(h_f - h_M) \quad . \quad (4)$$

where

$$X_R' = W_M/W_T$$

The quantity X_D/X_R is then computed by ratioing X_D to X_R , the riser exit quality. The latter is derived from a heat balance on the core. The carry-under is sensitive to W_T and, especially, to ΔT_{sub} ; therefore, any error in these measurements is reflected in the calculated rate of steam carry-under. In the event that liquid carryover occurs in the effluent steam, the heat balance must be modified and the following equation results:

$$\frac{X_D}{X_R} = \frac{(W_M/W_T)(h_f - h_M) - (h_f - h_{in})}{(Q/W_T) - (h_f - h_{in})}, \quad (5)$$

where

Q = reactor power, Btu/hr

W_M = feed-water flow rate, lb/hr

W_T = total recirculation flow rate, lb/hr

X_D/X_R = pounds steam in downcomer/pounds steam in riser.

F. Liquid Carryover in Effluent Steam

Data about the magnitude of the liquid carryover were obtained by three methods. The principal and most accurate method was a series of heat balances on the secondary and primary systems for heat dissipation. A heat balance with the secondary system establishes the true reactor power. The liquid carryover can then be computed by making a heat balance for the primary reactor system. In the case of EBWR, the heat balance was made for the Primary Reboiler, which has as its heat source the reactor steam:

$$X = \frac{W_{IE} h_{fg,IE}}{W_{PR} h_{fg,PR}}, \quad (6)$$

where

W_{IE} = intermediate heat exchanger flow rate, lb/hr

$h_{fg,IE}$ = heat of vaporization, intermediate heat exchanger, Btu/lb

W_{PR} = Primary Reboiler flow rate, lb/hr

$h_{fg,PR}$ = heat of vaporization, Primary Reboiler, Btu/lb.

Liquid-carryover data were also obtained from the discrepancy between the measured feed-water and steam-discharge flow rates. When liquid carryover occurs, more feed water is injected into the reactor than steam is withdrawn. This discrepancy is actually a measure of the rate of liquid carryover. The major uncertainty in these data is the rate of steam flow. With large amounts of water in the steam, the measured steam rate is undoubtedly in error. The magnitude of the error is unknown. However, the carryover data obtained in this manner check well with values obtained by the heat-balance method.

The third method consisted of taking steam samples from sampling probes located 6 in., $14\frac{1}{4}$ in., and $22\frac{1}{2}$ in. below the steam-discharge duct (see Fig. 5). The samples were analyzed for sodium-24 content. The results were compared with a sample of reactor water obtained from a sampling point in the downcomer. These data were used to establish carry-over gradients as a function of steam-dome height. Extrapolation to the height of the steam duct yields the actual liquid carryover.

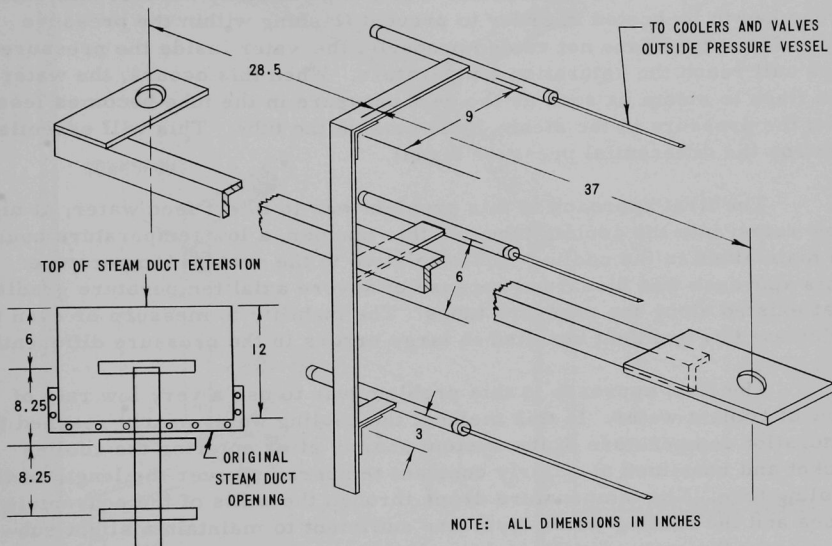


Fig. 5. Location of Liquid-carryover Sampling Probes in Steam Dome

III. INSTRUMENTATION

A. Differential Pressure Probes

The steam volume fraction was computed from measurements of static differential pressures that were made with specially designed probes. Ten probes were installed in the reactor. Measurement of the static pressure differential within the reactor was complicated by the fact that each probe had to be cooled in order to prevent flashing within the pressure taps. If the tubes are not cooled properly, the water inside the pressure taps will reach the saturation temperature. When this occurs, the water can flash to steam as soon as the head pressure in the tube becomes less than the pressure in the steam dome outside the tube. This will essentially destroy the differential pressure signal.

The first approach to this problem was to inject feed water, at high flow rates, into the cooling tube. In this manner, a low temperature could be maintained in the cooling jacket relative to the system temperature. This approach was discarded because of severe axial temperature gradients that existed along the pressure tubes. The inability to measure or even to calculate this gradient resulted in large errors in the pressure differentials.

The final approach to this problem was to use a very low rate of flow of coolant water. In this method, the cooling water nearly reached the saturation temperature of the system shortly after entering the cooling jacket and remained at a fairly constant temperature over the length of the cooling tube. The temperature drops through the walls of the concentric tubes and the cooling water layer are sufficient to maintain a slight sub-cooling up the entire length of the pressure tubes, eliminating the flashing problem and the difficulties caused by large axial temperature gradients. The design of the entire instrumentation complex was dictated primarily by these considerations.

The instrumentation complex is shown in Fig. 6. It consists of a single probe installed within the reactor and coupled with the measuring and read-out instrumentation. The probe was comprised of two $\frac{3}{16}$ -in. tubes which served as the pressure taps. The tubes were housed in a $\frac{9}{16}$ -in. tube through which the cooling water flowed. The cooling water discharged above the upper pressure tap. The temperature of the water in the leg between the pressure taps was thus maintained at slightly below the saturation temperature. Thermocouples were installed in several probes to monitor the cooling water. To protect the thermocouples from attack by steam and water, they were encased in $\frac{1}{8}$ -in. tubes and positioned within the larger, $\frac{9}{16}$ -in. tube.

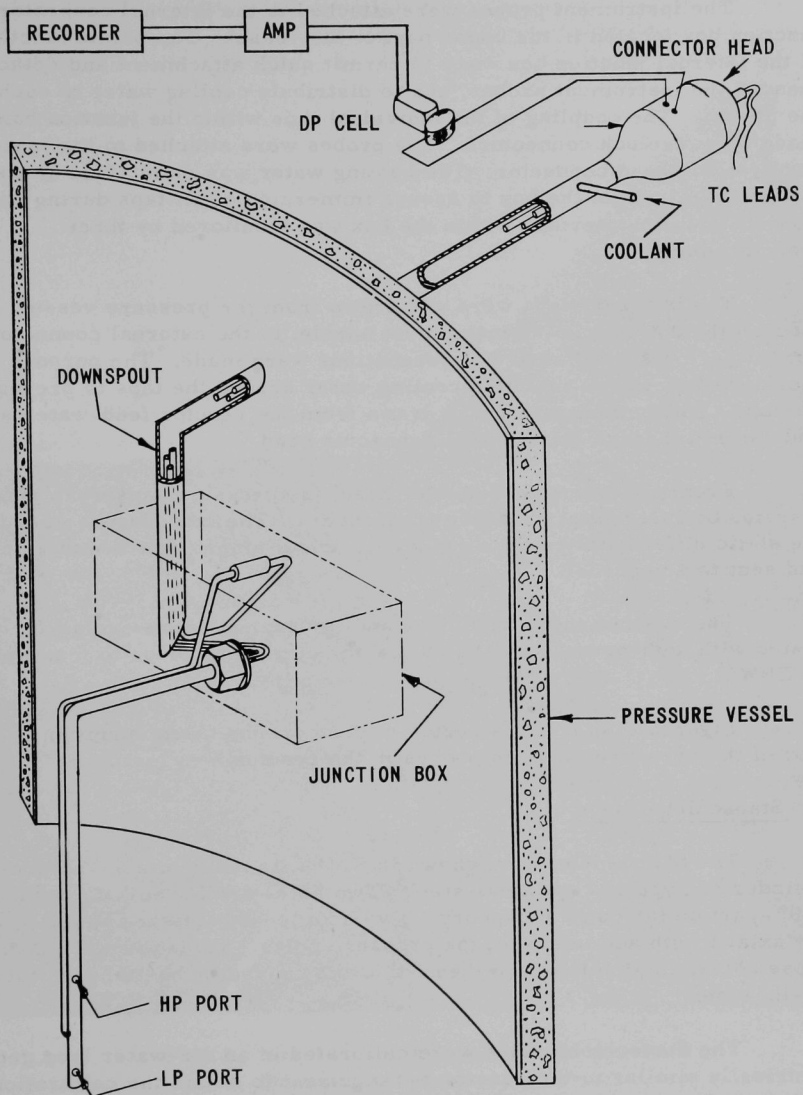


Fig. 6. Schematic of Single Probe Installed Inside Pressure Vessel and Coupled with Measuring and Read-out Instrumentation

The instrument probes were attached to the internal connector junction box located in the upper part of the vessel. The prime functions of the internal junction box were to permit quick attachment and detachment of the instrument probes, and to distribute cooling water to each of the probes. The coupling of the individual taps within the junction box was made by swagelock connectors. The probes were attached to the junction box by a bulkhead connector. The cooling water was maintained at a sufficient height within the box to assure immersion of all taps during operation. The water interface within the box was monitored by three thermocouples.

The pressure taps were withdrawn from the pressure vessel through the downspout and instrument nozzle, to the external connector head, where a second series of connections were made. The purpose of the downspout was to maintain cooling water around the taps to prevent flashing. The cooling water was drawn from the reactor feed-water supply and entered through the external connector head.

From the external connector head, the pressure taps were run to a series of differential pressure transducers. The transducers converted the static differential pressure to an electrical signal, which was amplified and sent to a recorder.

The experimental techniques and instrumentation were performance tested with high-pressure loops at reactor conditions prior to installation in EBWR.

Figures 7 to 12 are a series of photographs taken during installation of the pressure taps and probes in the reactor.

B. Stauschiebe Tubes

The Stauschiebe tube, shown in Fig. 4, is made of a $\frac{1}{2}$ -in.-diameter cylinder of Type 304 stainless steel. Two holes are bored $\frac{1}{4}$ in. deep and 180° apart on the outer periphery. Two additional holes are bored along the axial length and intersect the pressure holes. Tubing is welded into these holes, and the taps are then fed to the connector box through the $\frac{9}{16}$ -in. tube.

The Stauschiebe tubes were calibrated in an air-water loop geometrically similar to the reactor arrangement to obtain the calibration constant C, where

$$q = C V^2 / 2g \quad (7)$$

The calibration constant was calculated to be 1.456. As a further check, the Stauschiebe tube was used to measure the average flow rate in a 5-in.-ID pipe (by traversing across the diameter). The flow rate determined from an integration of the Stauschiebe flow profile checked within 1% of the flow rate measured by a calibrated orifice plate.

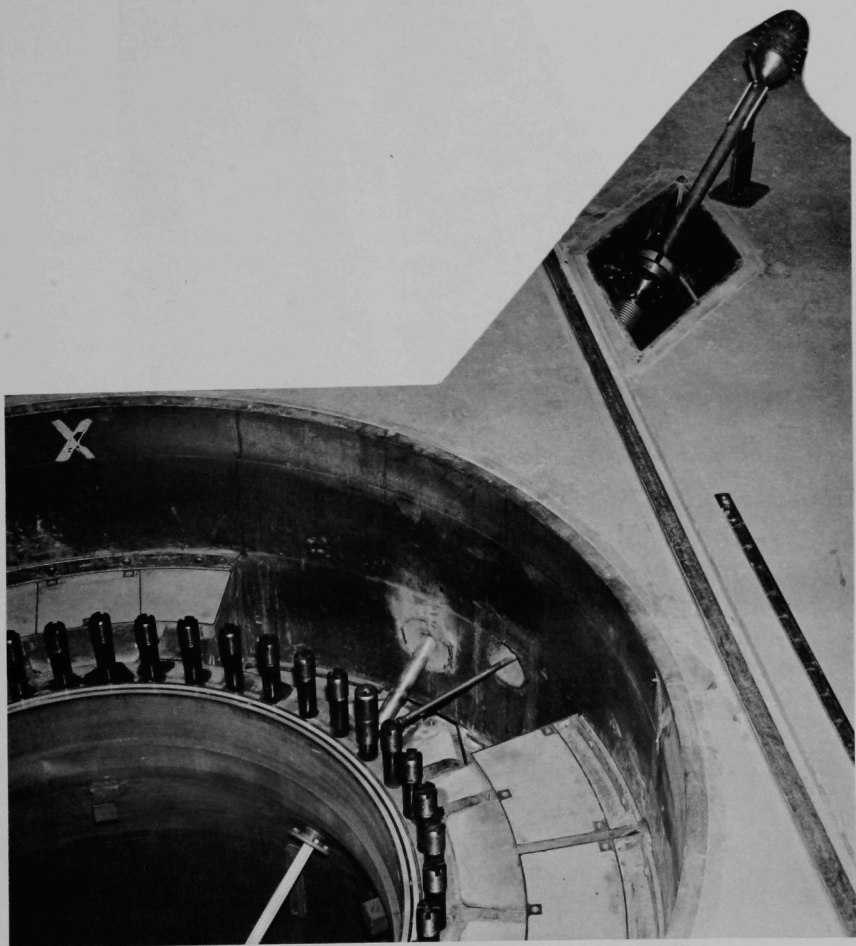


Fig. 7. Nozzle Penetration through Upper Shielding and Pressure Vessel

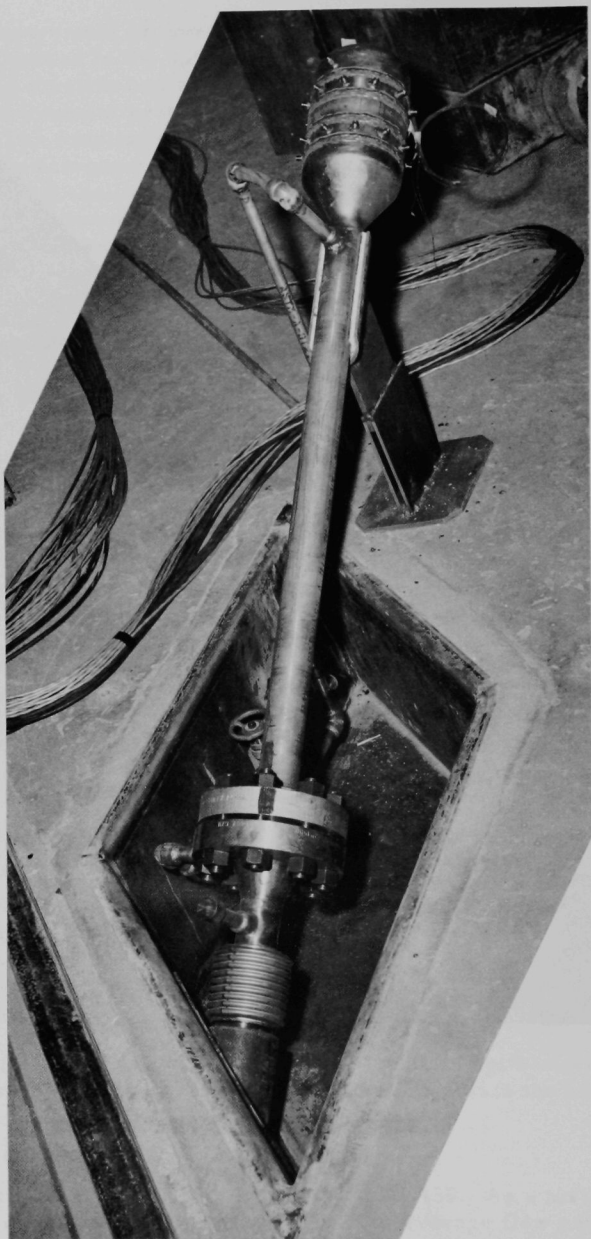


Fig. 8. Closeup View of External Connector Head

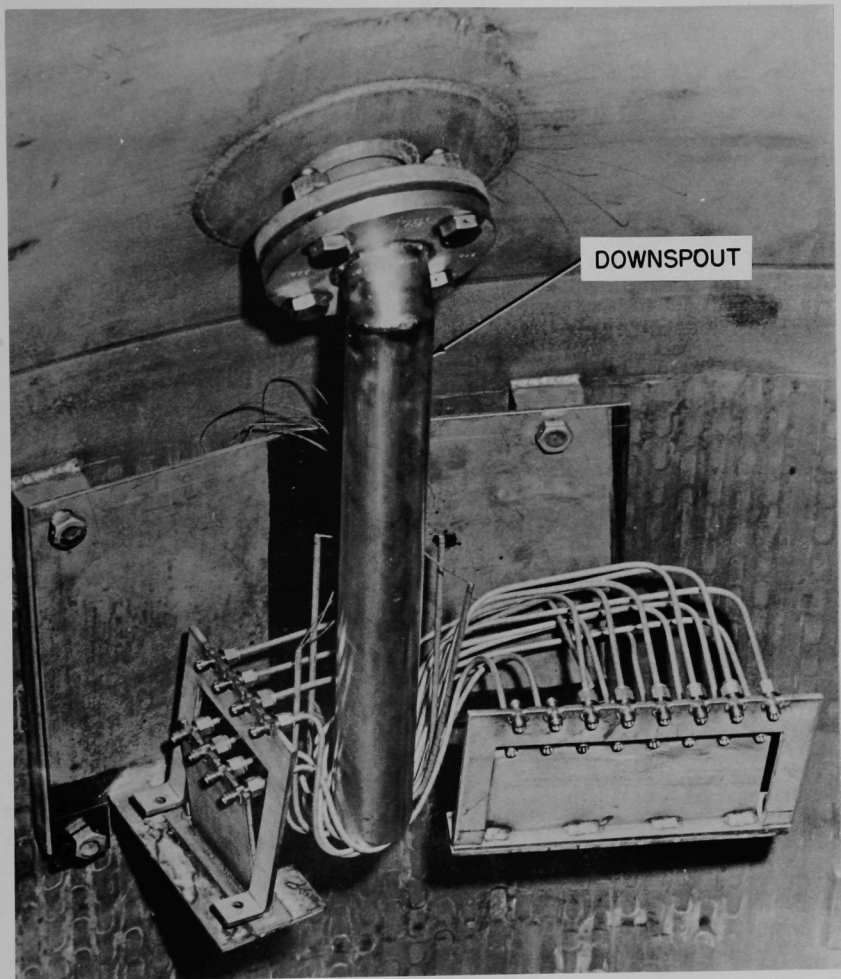


Fig. 9. Assembly of Pressure Taps to Manifold in Junction Box
(cover removed) within Pressure Vessel

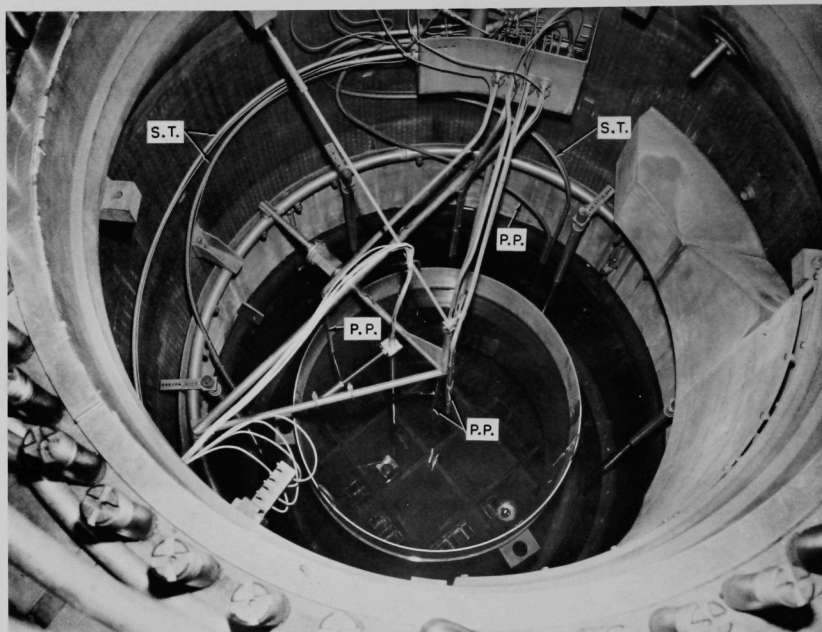


Fig. 10. Pressure Probes (P.P.) and Stauschiebe Tubes (S.T.) Installed in Pressure Vessel. Probe assembly is an integral unit which can be removed in 1 hr. Stauschiebe tubes (on vessel wall) were not removed during fueling, etc.

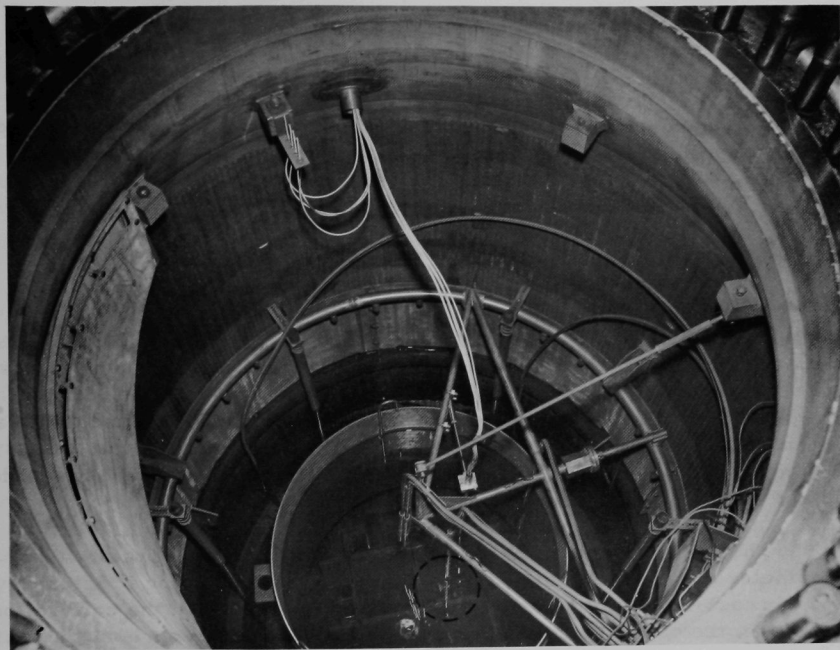


Fig. 11. Top: Thermocouple Installation in Steam Dome.
Bottom: Pressure Probes Leading to Core Region
and to Instrumented Fuel Subassembly (inset).

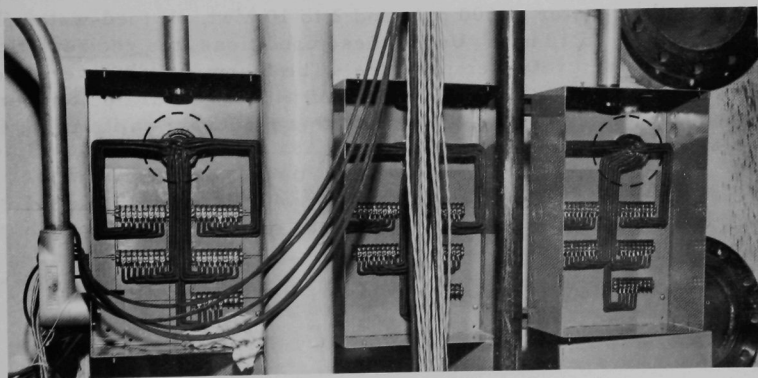


Fig. 12. Penetration of Instrument Leads to Terminal Boxes
Mounted on Outer Surface of Biological Shielding

C. Thermocouples

The subcooling measurements were made with insulated chromel-alumel thermocouples. Measurements of the temperature in the steam dome were made with grounded chromel-alumel thermocouples. The specifications for the thermocouples are tabulated below:

Outside diameter	0.0625 in.
Length	30 ft
Sheath	Inconel, 0.005 in. thick
Wire	Chromel-alumel, 30 AWG
Insulation	Magnesium oxide

The thermocouple leads from the reactor extended through a primary pressure seal (Conax fittings) at the blind flange of the instrument nozzle, a secondary pressure seal containing an amphenol connector, to an ice junction. Copper wire was run from the ice junction to the read-out. The thermocouple emf was recorded on a four-channel (0.25-sec) recorder and also read out on a potentiometer.

The thermocouples were calibrated initially in a laboratory hypsometer and, subsequently, in the reactor vessel. During the first few days of reactor operation, a significant change occurred in the calibration. Therefore, the calibration was performed periodically throughout the test program to maintain and to verify the accuracy of the subcooling measurements.

The procedure for calibration of the thermocouples in the reactor was as follows. The reactor water level was raised 2 to 3 ft above the riser. With the reactor at 600 psig and 2 to 10 Mwt, all feed-water flow was stopped for 5 to 10 min. Under these conditions, the recirculating water was at the saturated temperature. The thermocouples were then calibrated by comparing the measured emf with the saturated temperature corresponding to the pressure gauge. In this method of calibration, the reactor serves as a hypsometer.

IV. TEST PROGRAM

A. Preliminary

Upon completion of the probe installation, the reactor vessel was closed and subjected to a hydrostatic test. During this test, all pressure taps were bled (at the transducers) to remove any gases that may have accumulated in the vertical legs.

Preparatory to filling the probe system, the reactor was brought to a predetermined power level (5-10 Mwt). A small stream of reactor feed water was introduced through a $\frac{3}{16}$ -in. pressure tap directly into the internal junction box. As the water level in the junction box rose, the water entered the cooling annulus of the probes. Simultaneously, water started rising in the downspout, and gradually filled the nozzle and external connector head. The temperature of the external connector head and nozzle was measured by thermocouples attached to the surfaces of these components. The cooling water was monitored to prevent a rapid temperature transition which might cause excessive thermal stresses. When the connector was partially filled, it was vented to remove all traces of gases and to establish a solid water leg in the nozzle and downspout.

Another segment of the feed water was used to purge the pressure taps of any traces of gas accumulation. The purge flow was into the reactor and occurred simultaneously with the cooling of taps.

Upon completion of the purging operation, the instrument probes were allowed to reach thermal equilibrium prior to the start of the test program.

B. Test Series

The program comprised three series of tests. Test Series No. 1 was designed to check out the instrumentation and to obtain data on reactor performance with the new riser. The reactor operating conditions employed for the test series are listed in Table 1. The two make-up-water injection points (upper and lower feed-water rings) were used to study the effect of steam carryunder on a system behavior. A pressure of 300 psig was used to simulate operation at higher power density. The initial level of hot water, indicated in Table 1, was varied to study the effect on steam carryunder, and to obtain data on the difference between the indicated level of the water column and the true interface (void level) within the reactor vessel. The maximum reactor power level during this test series was 20 Mwt. Selected data from this test series are discussed in Section V. The complete data have been published in EBWR Test Report No. 105.⁽¹⁾

Table 1

REACTOR OPERATING CONDITIONS - TEST SERIES NO. 1

Power, Mw	Initial Saturated Hot Water Level above Riser, in.	Pressure, psi	Make-up-water-injection Point
5	3	600	Upper ring
5	3	600	Lower ring
10	3	600	Upper ring
10	3	600	Lower ring
15	3	600	Upper ring
15	3	600	Lower ring
20	3	600	Upper ring
20	3	600	Lower ring
5	12	600	Upper ring
5	12	600	Lower ring
10	12	600	Upper ring
10	12	600	Lower ring
15	12	600	Upper ring
15	12	600	Lower ring
20	12	600	Upper ring
20	12	600	Lower ring
5	3	300	Upper ring
5	3	300	Lower ring
10	3	300	Upper ring
10	3	300	Lower ring
15	3	300	Upper ring
15	3	300	Lower ring
20	3	300	Upper ring
20	3	300	Lower ring
5	12	300	Upper ring
5	12	300	Lower ring
10	12	300	Upper ring
10	12	300	Lower ring
15	12	300	Upper ring
15	12	300	Lower ring
20	12	300	Upper ring
20	12	300	Lower ring

Based on the data obtained, and prior to the start of Test Series No. 2, the top section (1 ft) of the riser was removed to increase the volume of the steam dome. Also, it was decided to inject feed water through the upper ring for the balance of the program. During Test Series No. 2, the saturated water level was maintained 7 in. above the top of the riser, the reactor power level was varied from 5 Mwt to 60 Mwt in ~5-Mw increments, and the pressure was constant at 600 psig. Test Series No. 2 ended with all control rods in the "full-out" position and with about 0.5 gm boric acid/gal water (equivalent to ~0.5% k) remaining in the reactor at 60 Mwt.

In order to increase the reactivity and, hence, to attain higher power levels, additional boron strips were removed from the spike fuel elements. The destripping introduced an estimated additional 2.2% k. Test Series No. 3 was then run at power levels ranging from 55 Mwt to 100 Mwt.

V. DISCUSSION OF RESULTS

A broad generalization of the results of the test program with EBWR is as follows:

The performance characteristics of EBWR are governed directly by steam carryunder in the downcomer, liquid carryover in the effluent steam, and, indirectly, by the location of the true water-steam interface in the vessel.

The effect of steam carryunder and liquid carryover on reactor performance is reflected in the core inlet subcooling and, hence, mean core moderator density. As the magnitude of the steam carryunder increases, the subcooling and moderator density decreases, since the mean steam volume fraction increases. The effects are reversed with liquid carryover. In order to maintain a constant liquid inventory, an excess of cold feed water is injected into the reactor. This increases the reactor subcooling and, hence, the reactivity. The excess water is expelled in the effluent steam. The carryover phenomenon radically alters the performance characteristics of the reactor. Under these conditions, it is not a normal, direct-cycle, boiling water reactor; in a sense, it becomes a natural-circulation, dual-cycle reactor. The steam carryunder and liquid carryover are very sensitive to the true two-phase mixture interface within the reactor vessel. As the interface is lowered, the carryunder rises rapidly and the carryover decreases. As the interface is raised, the effects are opposite: carryunder decreases and carryover increases.

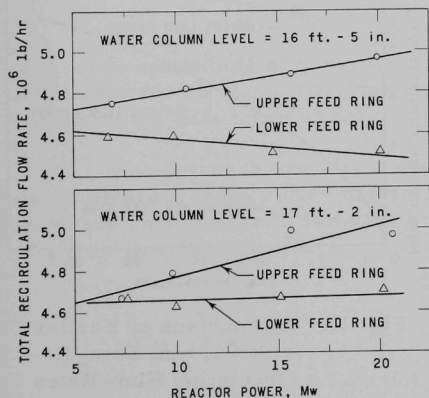


Fig. 13. Total Recirculation Flow Rate as a Function of Reactor Power at 600 psig for Two Water Column Levels

A. Total Reactor Recirculation Flow Rates

Figures 13 and 14 are plots of the recirculation flow rates as a function of power during Test Series No. 1. For this series of tests, the top of the riser corresponded to a water column level of 17 ft 3 in. The data obtained are presented to illustrate the effect of the feed-water-injection point on the recirculation flow rate.

The magnitude of the flow rates is in agreement with an earlier core analysis and extrapolation from EBWR data. The analysis indicated that a two-fold increase in flow rate could be expected with the additional

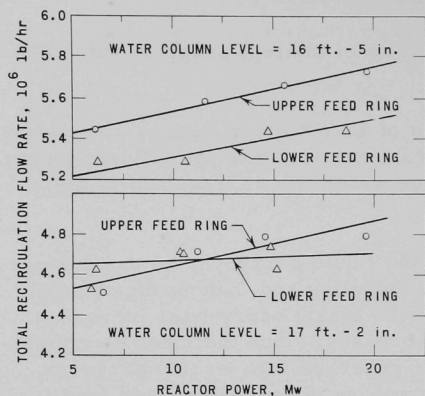


Fig. 14. Total Recirculation Flow Rate as a Function of Reactor Power at 300 psig for Two Water Column Levels.

When the make-up water was injected in the lower feed ring, reactor operation approximated the equilibrium state. Under the conditions of power, water column height, and pressure studied, the recirculation flow rate was $\sim 4.7 \times 10^6$ lb/hr (see Figs. 13 and 14). The exception was the series of runs at 300 psig with an initial water level of 16 ft 5 in. (see Fig. 14).

The equilibrium flow rate corresponds to a velocity of 1.2 ft/sec in the upper downcomer region. This behavior was anticipated. With the make-up water injected in the lower feed-water ring, the net driving head of the reactor is essentially $L_R(\bar{\rho}_D - \bar{\rho}_R)$. Since the voids do not collapse until they reach the lower injection point below the 7-ft riser, one would expect the reactor to stabilize at a total flow just above the critical

riser height. However, the rate of increase of the recirculation velocity with power and decreasing pressure was not as large as predicted by the analysis.

Figure 15 shows a comparison of the measured flow rates with earlier EBWR data(2) as projected to a full-size core. The measured data are representative of the tests at 600 psig, with make-up water injected in the upper feed ring. At the lower power levels, the expected flow increase was achieved, but the rate of increase with power was much smaller. Tentatively, the lower rate of increase of flow is attributed to loss of subcooling and, hence, increased frictional resistance in the core resulting from steam carryunder in the downcomer.*

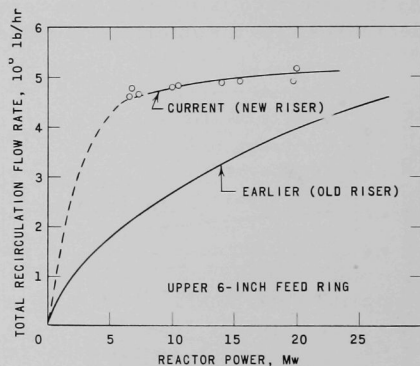


Fig. 15. Comparison of Earlier with Current Total Recirculation Flow Rates at 600 psig.

*This observation is subject to corroboration by an extensive thermal-hydraulic analysis of the reactor. The results will be published in a separate report.

value for the initiation of steam carryunder. When the critical value is exceeded and steam carryunder commences, small amounts of steam produce large steam volume fractions, since the relative velocity of the two phases is very near zero. This immediately tends to reduce the net driving head by decreasing the density in the downcomer ($\bar{\rho}_D$). Thus, the reactor reaches an equilibrium recirculation flow rate. The measured velocity of 1.2 ft/sec in the reactor downcomer agrees very well with laboratory loop data.⁽³⁾ The latter shows that the threshold velocity for the initiation of carryunder at 600 psig is ~ 1.3 ft/sec.

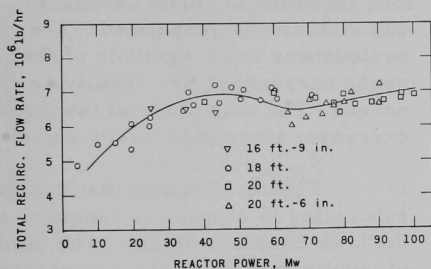


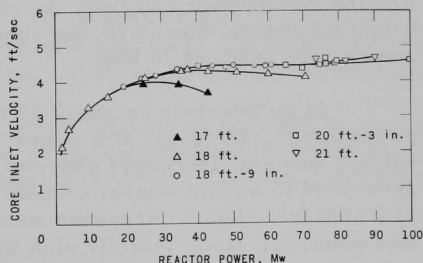
Fig. 16. Total Recirculation Flow Rate as a Function of Reactor Power at 600 psig and Various True Mixture Interface Levels.
112-2608

where the magnitude of carryover is large and the subcooling near zero, due to excessive steam carryunder, and the flow rates are lower, as depicted by the data taken at an interface height of 16 ft.

These trends are also shown in Fig. 17. The core inlet velocity data were obtained from Potter meters installed in an instrumented fuel assembly near the core center.* Note the branching of the velocities as a function of the true interface height.

Fig. 17

Core Inlet Velocity as a Function of Reactor Power and Various True Mixture Interface Levels.
112-2616



*G. F. Popper, ANL, private communication.

The measured recirculation flow ranges correspond to a velocity range of 1.2 ft/sec to 1.8 ft/sec in the upper downcomer area.

B. Subcooling

Subcooling is perhaps the most important measurable reactor parameter since it reflects the effects of carryover and carryunder, and the variation of other parameters such as recirculation flow, interface height, etc. The effects of the vapor carryunder, liquid carryover, and true interface height are clearly evident in the subcooling "map" of EBWR (see Fig. 18).

The inception of liquid carryover can virtually be pinpointed. The seriousness and magnitude of the vapor carryunder are readily apparent. The magnitude of the liquid carryover also can be easily deduced.

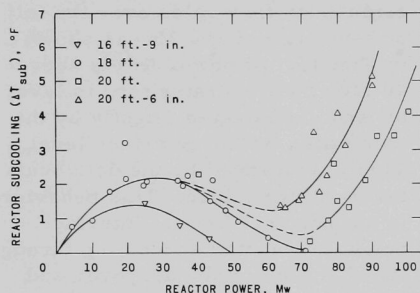


Fig. 18. "Map" of Reactor Subcooling as a Function of Reactor Power and Various True Mixture Interface Levels.

112-2619

continuously with power if no steam carryunder is present. At zero subcooling, the carryunder is 34.6 w/o.

As the interface height is increased to 18 ft, the subcooling increases slightly and the peak occurs at a higher power level. The behavior is due to the fact that the carryunder is a function of the interface height. For the same power and flow, the carryunder decreases as the interface height increases; therefore, the subcooling is greater. The subcooling becomes zero at about 70 Mw.

At an interface height of 20 ft, the trend is the same in the lower power range. However, at a power level of approximately 70 Mw, the subcooling suddenly increases sharply. The height of the steam dome has decreased to a point where, coupled with a superficial dome vapor velocity of 1.25 ft/sec, liquid carryover occurs. As the power is increased beyond this point, the vapor velocity also increases, and the quantity of liquid carried over rises rapidly. The identical trend is seen in the data taken

Figure 18 shows that reactor subcooling is extremely sensitive to the true interface height. The family of curves merges at the low reactor powers. At an average interface height of 16 ft 9 in., the subcooling increases slightly with power, peaks at about 20 Mw, and then diminishes rapidly toward zero at about 50 Mw. This pattern of subcooling is a result of the steam carryunder in the downcomer. For normal reactor operation, the subcooling increases

at an interface height of 20 ft 6 in. The difference is that the subcooling is again slightly higher, and the point of carryover is reached at a lower power level. This is due to the reduced steam dome height.

The increase in reactor subcooling due to carryover can be predicted by making a heat balance for the downcomer with the aid of Eq. (5). The results of this analysis are shown by the dashed line in Fig. 19. The value of X_D/X_R (carryunder) was obtained by extrapolation from the lower powers.

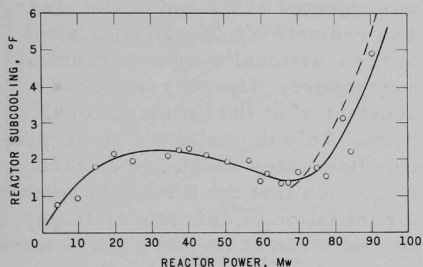


Fig. 19

Measured Reactor Subcooling as a Function of Reactor Power. Increase in subcooling at 70 Mw is due to liquid carryover. Dashed curve shows subcooling predicted from measurements of liquid carryover

Confidence in the measured subcooling and recirculation flow rates was gained from the following considerations:

(1) Assuming no steam carryunder in Eq. (4), the recirculation flow rate W_T was computed with the use of the subcooling data and compared with the hydrodynamic analysis of EBWR. The estimated maximum total flow rate at 100 Mw is $\sim 12 \times 10^6$ lb/hr. In general, the calculated flow rates using the heat balance greatly exceed this value, even at the low power level (see Fig. 20). Thus it must be concluded that the heat balance flows are false and the low subcoolings are a result of carryunder.

(2) The rate of change of flow with power, as seen in Fig. 20, is too great to be justified by any reasonable hydrodynamic analysis.

(3) The slip ratios in the riser, which were computed from the measured flow rates, check well with correlations developed from laboratory loop studies. Had the heat balance flow rate been used, the majority of the slip ratios would have been less than one. This is a physical impossibility.

(4) Under reactor conditions where little or no carryunder is expected (e.g., 5 Mw) and make-up water is injected through the lower feed ring, the measured flow rates check well with the heat balance flow rates.

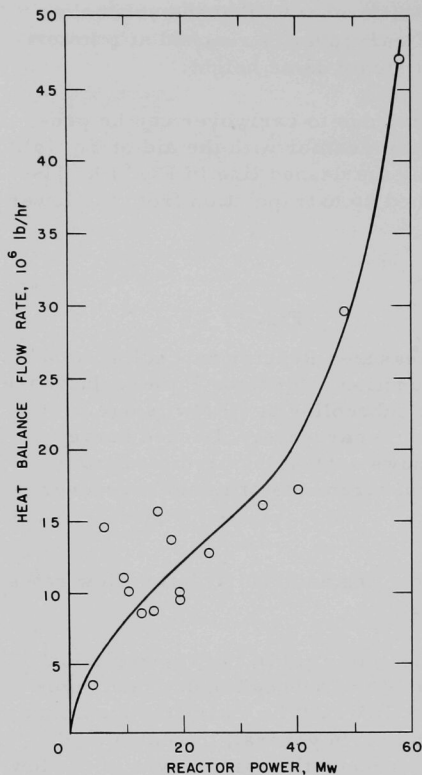


Fig. 20. Heat Balance Flow Rates as a Function of Reactor Power.

of 34.6% (which corresponds to the point where all subcooling is eliminated) is due to the occurrence of liquid carryover.

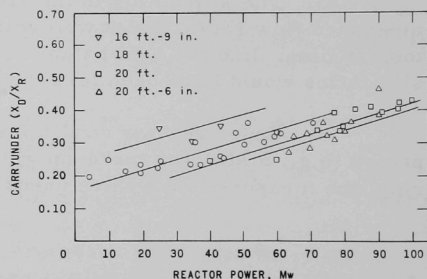
C. Vapor Carryunder

The vapor carryunder in the reactor was calculated from a heat balance, through use of the measured subcoolings and flow rates, as discussed previously. The steam carryunder as a function of power and interface height is plotted in Fig. 21. For these runs, the make-up water was injected at the top of the riser. The ordinate X_D/X_R is equivalent to the fractional weight-percent of carryunder. The carryunder is substantial at the lower powers, ~20%. This is due to the recirculation flow rates which are of such magnitude that the threshold velocity for initiation of carryunder is exceeded, even at the very low powers. As mentioned previously, the data indicate that the threshold velocity for the initiation of carryunder is 1.3 ft/sec. As the power is increased, the carryunder increases gradually to a value of ~40% at 100 Mw for an intermediate liquid interface height, that is, 40 w/o of all steam generated in the core is being entrained in the downcomer. At 100 Mw, the average velocity in the downcomer was 1.8 ft/sec. The fact that the carryunder has exceeded the theoretical limit

Fig. 21

Steam Carryunder as a Function of Reactor Power and True Mixture Interface Levels.

112-2617



The magnitude of vapor carryunder in the downcomer is somewhat startling, but corroborating data are available. As an example, evidence of the excessive carryunder was obtained from physics analysis of the core for average steam volume fractions (see Fig. 22). Based on hydrodynamic analysis of the core and an assumption of no carryunder, the estimated void content was 12% at 60 Mw. This is in sharp contrast with the value of 27% derived from measured physics parameters of the core. The latter value, which corresponds to 5% k, was expected at 100 Mw.

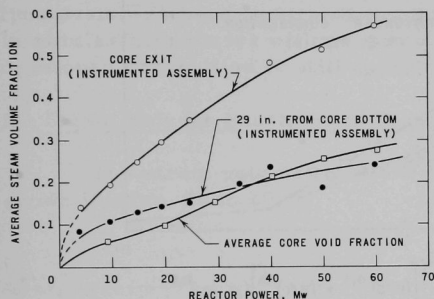


Fig. 22. Calculated Average Steam Volume Fraction in Core as a Function of Reactor Power.

velocity. The overall effect was that the percent of carryunder continued to increase with power.

The data were compared with the carryunder correlations developed from the loop studies. The results are plotted in Figs. 23 and 24. In Fig. 23, the data appear to deviate from the correlation. Actually, the slope of the line drawn through the data, when plotted as X_D/X_R versus the functions $f(V_g, V_{ent}, G, \sigma, \mu, H, D, \rho_f, \rho_v)$, differs from the loop-developed correlation. This can be attributed to one significant difference between the reactor data and the loop data. In the reactor, the steam carried under is immediately subjected to quenching, since the cold feed water is injected at the top of the riser. Thus, the true liquid velocity $[V_D/(1 - \alpha)_D]$ at the top of the downcomer is lower than would prevail if no quenching occurred. For making the comparison shown in Fig. 24, the entrainment ratio V_g/V_{ent} was calculated under the assumption of no quenching. The slip ratios were calculated from the following equation:⁽³⁾

$$\frac{V_g}{V_L} = 0.63 (Fr)^{0.4} \left(\frac{x}{1-x} \frac{\rho_f}{\rho_v} \right)^{0.2} \quad (8)$$

The slip ratio was then used to calculate the void fraction in the downcomer (α_D). The calculated values were much greater than the measured values of

Laboratory loop studies⁽³⁾ showed that, as power is increased for a fixed recirculation velocity, the percent of carryunder decreases, reaches a minimum, and then begins to increase. This sequence did not occur in the reactor since the recirculation velocity continued to increase slightly with power. Once the threshold velocity for carryunder is passed, substantial increases in carryunder occur with small increases in velocity. In EBWR, the expected decrease of carryunder with increasing power apparently was nullified by the increase in the recirculation

the steam volume fraction due to the quenching which occurs in this region. The overall effect was to make the entrainment ratio V_g/V_{ent} and, hence, the functions $f(V_g, V_{ent}, \dots \rho_v)$ abnormally low. The quenching is, therefore, believed to be the reason for the deviation of the data from the correlation.

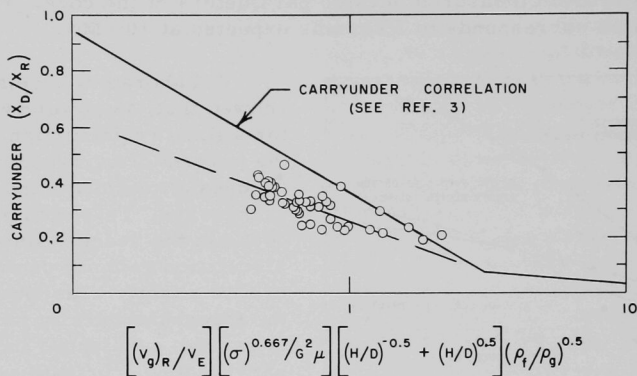


Fig. 23. Comparison of Carryunder Data with the Correlation, Using Calculated Steam Volume Fraction.

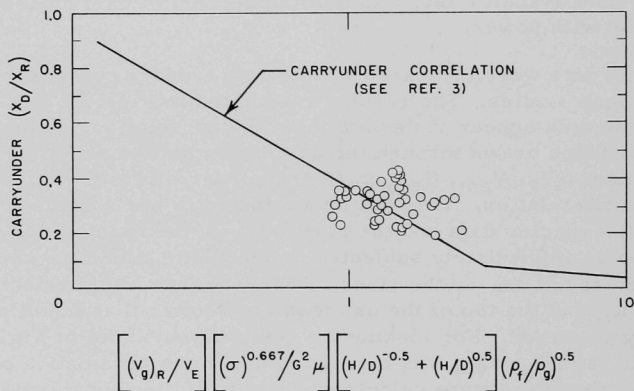


Fig. 24. Comparison of Carryunder Data with the Correlation, Using Measured Steam Volume Fraction.

An attempt was made to substantiate this by re-evaluating the entrainment ratio V_g/V_{ent} and the functions $f(V_g, V_{ent}, \dots \rho_v)$ by using the measured steam volume fractions with quenching in the top part of the downcomer.

These data are compared with the correlation in Fig. 24. The data shift over and fall in line with the correlation, but the scatter is much greater. The scatter may be due to inaccuracies in determining the steam volume fraction in the upper part of the downcomer (Probe C-2) because of the quenching process and the high degree of turbulence created by the injection of the cold feed water in the form of high-velocity jets.

In summary, the correlation based on the actual reactor data is probably more appropriate for estimating the vapor carryunder in EBWR-type systems where quenching occurs in the upper part of the downcomer. In similar geometries with no quenching it appears that the previously developed correlation is still applicable.

D. Steam Volume Fractions in Riser and Downcomer

The steam volume fractions in the riser and the downcomer are shown in Figs. 25 to 29.

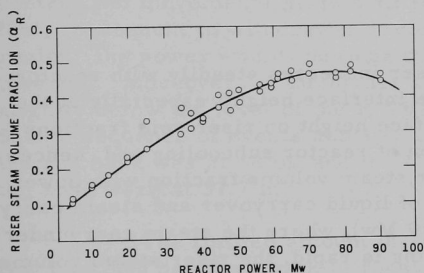


Fig. 25. Steam Volume Fraction in Riser as a Function of Reactor Power.

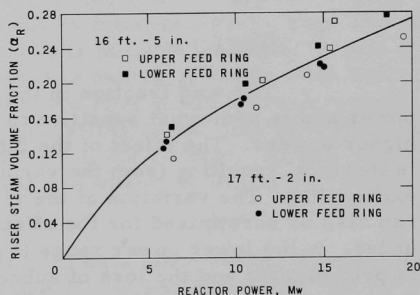
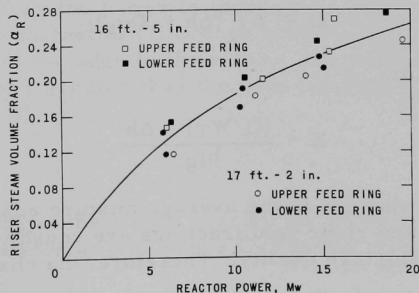


Fig. 26. Steam Volume Fraction in Center of Riser as a Function of Reactor Power at 300 psig.

Fig. 27

Steam Volume Fraction at Periphery of Riser as a Function of Reactor Power at 300 psig.



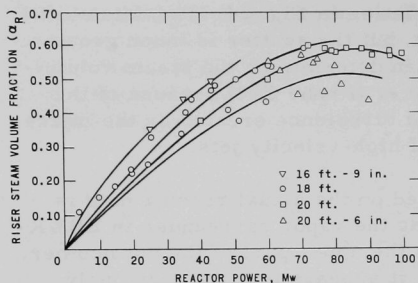


Fig. 28. Steam Volume Fraction in Center of Riser as a Function of Reactor Power at 600 psig and Various True Mixture Interface Levels.

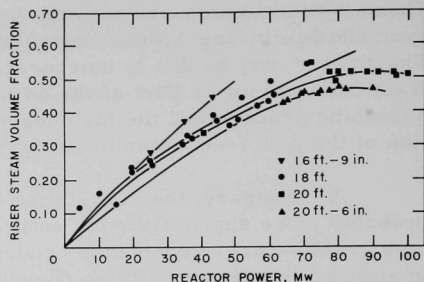


Fig. 29. Steam Volume Fraction at Periphery of Riser as a Function of Reactor Power at 600 psig and Various True Mixture Interface Levels.
112-2614

1. Riser

The void fraction in the riser increases steadily with reactor power and is somewhat sensitive to the interface height, especially at the higher powers. The effect of the interface height on riser void fractions is indirect, resulting from the variation of reactor subcooling and, hence, exit quality. The variation of the riser steam volume fraction with power can also be scrutinized for the effects of liquid carryover and steam carryunder. In the lower power range (20-50 Mw), where the steam carryunder is predominant and the loss of subcooling is rapid, the riser steam volume fraction rises rapidly. In the middle power range (60-80 Mw), where the threshold of liquid carryover is reached, the void fraction tends to level off. In the region of very high power (>80 Mw), the steam volume fraction tends to decrease. This behavior in the high-power region is expected since the subcooling is increasing rapidly with power. An indication of the change in the void content can be gained from a simple heat balance:

$$Q = W_T (\Delta h + X h_{fg}) \quad (9)$$

or

$$X = \frac{(Q/W_T) - \Delta h}{h_{fg}} \quad , \quad (10)$$

where X is the average mixture quality at the core exit. The average core and riser void fractions are roughly proportional to the average exit core mixture quality. Therefore, the change in quality and, hence, change in

voids was computed over the power level intervals: 70-80 Mw, 80-90 Mw, and 90-95 Mw. The results are as follows:

$$\frac{\alpha(80 \text{ Mw})}{\alpha(70 \text{ Mw})} \sim \frac{X_e(80 \text{ Mw})}{X_e(70 \text{ Mw})} = 1.062$$

$$\frac{\alpha(90 \text{ Mw})}{\alpha(80 \text{ Mw})} \sim \frac{X_e(90 \text{ Mw})}{X_e(80 \text{ Mw})} = 1.02$$

$$\frac{\alpha(95 \text{ Mw})}{\alpha(90 \text{ Mw})} \sim \frac{X_e(95 \text{ Mw})}{X_e(90 \text{ Mw})} = 0.97$$

These figures, although not precise, clearly indicate the decreasing rate of void increase as the power is increased. Between 80 and 90 Mw, there is virtually no change in exit quality; hence, the core and riser void fractions would tend to remain nearly constant. Between 90 and 95 Mw, it appears that the void content actually decreases; hence, the reactivity would increase. This behavior is shown in Fig. 25 and was corroborated by the control rod movements made over this power interval. These data indicate that, consequent to withdrawal of control rods to increase power in this region, the power would continue to increase unless the rods were re-inserted. Moreover, at the higher power, the rods would be re-inserted slightly below the level of the rod bank prevailing at the time of withdrawal. Such a sequence of events actually occurred in the reactor. At 88.6 Mw, the rod bank was at 38 in. and the central rod was at 40 in.; at 90.7 Mw, all the rods were at 37.7 in.

The limited amount of riser void data taken during Test Series No. 1 (at 300 psig) is shown in Figs. 26 and 27. It was found that the 300-psig void data fit the 600-psig curve when plotted at two times the power. This tends to substantiate previous analysis which showed that operation at a given power at 300 psig was equivalent to operation at approximately twice the power at 600 psig.

The data also indicate a definite phase distribution in the riser. This distribution becomes more skewed as the power is increased. For example, in Figs. 28 and 29 there is a substantial difference between the void fraction measured at the center and the edge of the riser. The void fraction in the center (Probe A) is always greater than the void fraction near the periphery of the riser (Probe B).

2. Downcomer

Data on the rate of quenching of the steam carried under were obtained from Probe D in the lower downcomer and Probe C-2 in the upper downcomer (see Fig. 3).

An insight into the collapse-rate pattern of the steam bubbles can be gained from a rough theoretical analysis of the problem. If it be assumed that the collapse of a vapor bubble in a subcooled liquid is governed primarily by the rate of heat transfer at its surface during the major fraction of its life time, the following expression can be obtained:

$$\left(\frac{R}{R_i}\right)^{5/4} = 1 - 1.275 (\text{Pr}_f)^{0.5} \left[g \frac{R_i^3}{\nu_f^2} \frac{1}{\text{Ca}_d} \left(1 - \frac{\rho_v}{\rho_f}\right) \right]^{0.25} \frac{\rho_f}{\rho_v} \frac{c_f \Delta T_{\text{sub}}}{h_{fg}} \frac{k_f \Delta t}{R_i^2} \quad (11)$$

Ruckenstein's theoretical expression for the bubble Nusselt number is used,⁽⁴⁾ and the assumption is made that the bubble is moving in a quiescent fluid. Undoubtedly, in a highly turbulent region the collapse rate of a bubble would be much higher than that predicted by Eq. (11). However, the qualitative effect of subcooling on the collapse rate is considered fairly accurate.

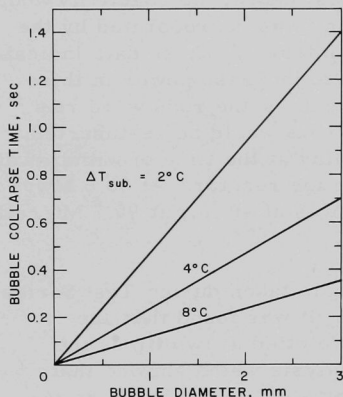


Fig. 30. Effect of Subcooling on Bubble Collapse Time.

112-2612

Figure 30 shows the results of some calculations which illustrate the strong effect of subcooling on the collapse rate of bubbles of various diameters. As the subcooling increases, the time required to collapse the vapor bubble decreases. Thus, at the top of the downcomer, where the cold feed water is injected, the subcooling is maximum, the collapse rate is also at a maximum, and one would expect a sudden large drop in the void content.

In an EBWR-type reactor, where cold feed water is injected into the downcomer, the subcooling would vary from one degree at ~10 Mw, to ~12° at 100 Mw, assuming no carryunder. At low powers, the collapse rate is at a minimum; thus, a large quantity of steam carryunder would reflect a high steam volume fraction. As the power increases, the theoretical subcooling increases and thus the bubble collapse rate increases. Hence, for the same amount of steam carryunder, the steam volume fraction would be lower. In the very high power range (>75 Mw), where excess cold water is injected to the liquid carryover, the collapse rate is even greater; and despite maximum carryunder, a low steam volume fraction would be expected. Moreover, because of liquid carryover, the steam volume fraction would decrease with power. Figure 31 illustrates the type of void pattern expected in the upper region of the downcomer. In the lower downcomer region, virtually all the steam voids would

be condensed because of the transient time involved. This is especially true in the very high power range where an excess of feed water is injected.

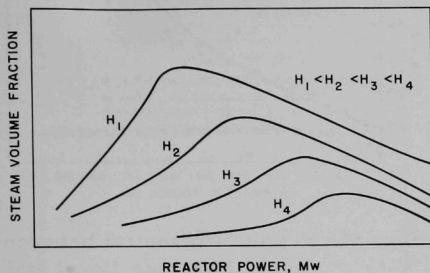


Fig. 31. Steam Volume Fraction as a Function of Reactor Power, Showing Void Pattern Expected in Upper Region of Downcomer.

112-2607

power is increased, the steam volume fraction decreases in a manner similar to that predicted by theory. In the lower region of the downcomer, the steam volume fraction is virtually zero under all conditions (see Fig. 33).

E. True Liquid Level

The difference between the true fluid interface level in the reactor and the level as indicated by the water column is shown in Fig. 34. The height differential is a result of the steam voids present in the core, riser, downcomer, and the "bubble bed" above the riser. The voids that are formed in the reactor core and riser, and entrained in the downcomer, displace an equal volume of water; this causes an increase in the mixture height. The water level above the riser is, in turn, further expanded by the vapor flowing through it; this creates a two-phase mixture or "bed." As shown in Fig. 34, the discrepancy between the two levels can be quite large.

The downcomer steam volume fraction data obtained from Probes C-2 and D are shown in Figs. 32 and 33, respectively. At first glance, the data appear to be erratic, with excessive scatter. However, upon closer scrutiny some interesting trends can be deduced which apparently substantiate the foregoing analysis. The major deterrent to establishing conclusive patterns is that the data were not taken over the entire power range at a fixed interface height. However, as shown in Fig. 32, the steam volume fraction in the upper region of the downcomer is maximum at the lowest powers and lowest interface heights. As the interface height is raised and the

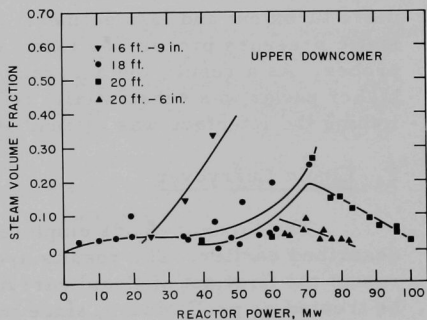


Fig. 32. Steam Volume Fraction in Upper Region of Downcomer as a Function of Reactor Power and Various True Mixture Interface Levels.

112-2609

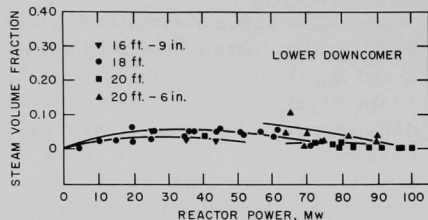


Fig. 33. Steam Volume Fraction in Lower Region of Downcomer as a Function of Reactor Power and Various True Mixture Interface Levels.
112-2606

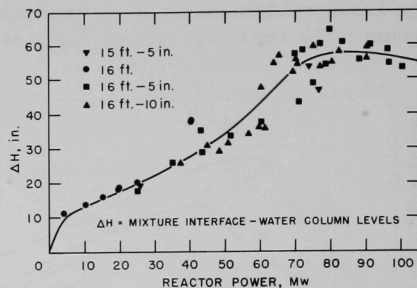


Fig. 34. Height Differential between Actual Interface Level and Water Column Level as a Function of Reactor Power and Various True Mixture Interface Levels.
112-2618

The height differential is primarily a function of reactor power and increases as the power is increased. In the very high power range where liquid carryover occurs, the height differential levels off and begins to decrease. This is a result of the sudden increase in subcooling and, hence, decrease in core and riser void content. The scatter of the data increases with power. This is probably due to the fact that the interface becomes more turbulent and less defined. Also, the distance between the upper two static pressure probes was twice as large as that between the lower two probes. As a result, the accuracy for the interface determination at the higher power was substantially reduced. The maximum error in establishing the interface was estimated to be 9 in.

F. Liquid Carryover

The three methods employed to determine the liquid carryover were described earlier. The results are compared in Fig. 35. These data represent the first set of liquid carryover measurements made. They are to be treated as preliminary, since the true mixture interface levels were not determined at this time. However, these data do serve to point up the agreement among the three techniques.

The data obtained from the sampling probes were limited, owing to time considerations and termination of the program. However, some interesting trends are illustrated in Fig. 36, in which the percent carryover is plotted as a function of the distance above the vapor-liquid interface. A family of curves is obtained for varying superficial vapor velocities (powers); hence, it is readily apparent that carryover rates cannot be expressed in

terms of superficial vapor velocities alone. The height of the steam dome must also be specified. As the actual steam dome height decreases, the carryover increases rapidly.

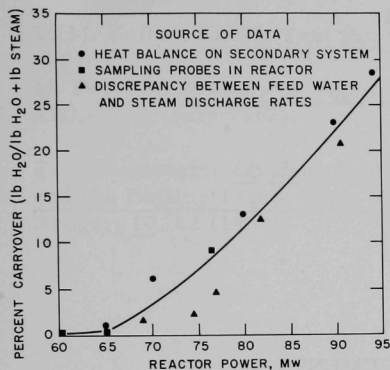


Fig. 35. Percent Liquid Carryover as a Function of Reactor Power, Showing Comparison of Data Obtained from Three Sources

112-2615

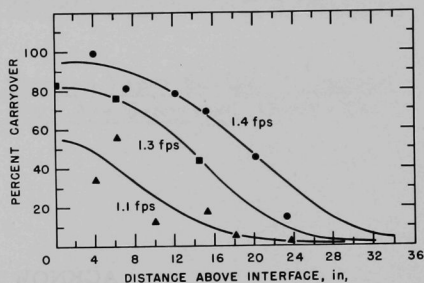


Fig. 36. Percent Liquid Carryover as a Function of Distance above Vapor Interface for Various Superficial Vapor Velocities

112-2610

The liquid carryover data derived by the heat balance technique are the most accurate and probably of greatest interest since they represent the actual amount of water carried over into the Primary Reboilers. As illustrated in Fig. 37, the initiation of carryover occurs at different power levels for different interface heights. At 60 Mw, the carryover starts at a superficial velocity of 1.1 ft/sec, with a steam dome height of 30 in. As the steam dome height increases, the superficial vapor velocity required to initiate large amounts of carryover also increases.

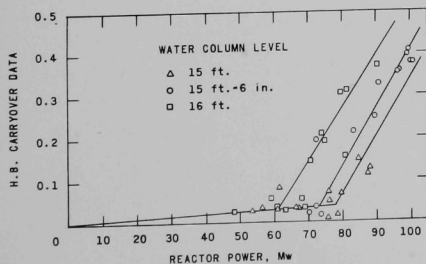


Fig. 37

Liquid Carryover as a Function of Reactor Power and Various Water Column Levels. (Data from heat balance on primary reboiler.)

112-2613 Rev.

A comparison of the data derived from the reactor with data obtained under static conditions (no fluid recirculation) shows that the magnitude of the carryover is larger for the same condition of vapor velocity and dome height. The amount of liquid carryover measured in the reactor was much larger than had been expected.

ACKNOWLEDGEMENTS

The authors wish to express their appreciation to the following members of the Heat Engineering Section: G. Rezek, who aided in the initial design and construction states; M. Gats, who was most helpful during the construction and installation stages; H. Niemoth, who laid out and installed most of the electrical equipment; G. Lambert, who worked on many facets of the project and who helped in the reduction of the vast amount of data; and Joe Kemp, Bill Brewer, Dan Quinn, and Elmer Gunchin, for their general assistance throughout the test program.

REFERENCES

1. Compilation of EBWR Test Reports: 40 Mwt to 100 Mwt, ANL-6703 (to be published).
2. V. M. Kolba, EBWR Test Reports, ANL-6229 (Nov 1960), p. 295.
3. M. Petrick, A Study of Vapor Carryunder and Associated Problems, ANL-6581 (July 1962).
4. E. Ruckenstein, On Heat Transfer between Vapor Bubbles in Motion and the Boiling Liquid from Which They Are Generated, Chem. Eng. Progr., 10, 22 (1959).

APPENDIX
TABULATIONS OF DATA

Table A-1

SUMMARY OF REACTOR DATA

Run No.	Power, Mw	Water Column, ft.-in.	True Level, ft.		ΔH (Avg), in.	ΔT_{sub-Q}	W _T , 10 ³ lb/hr	Riser		Downcomer		Void Fraction in Bubble Bed		Quality			Superficial Velocity, fps			f**	
			Center	Edge				σ_A Center	σ_B Edge	σ_C-1 Before	σ_C-2 During Quenching	σ_D After	σ_F-1	σ_F-2	X _D	X _R	X _D /X _R	V _D	V _R		V _S
101	4.07	16-10	17.92	17.57	10.90	0.75	4.8852	0.1040	0.1138	0.0260	0.0260	0.0583	-	0.1170	0.00051	0.00271	0.1890	1.275	2.316	0.068	1.870
102	9.97	16-10	18.10	17.82	13.50	0.95	5.4921	0.1495	0.1560	0.0520	0.0312	0.0810	0.8125	0.1040	0.00167	0.00700	0.2389	1.433	2.604	0.169	1.650
103	19.60	16-10	18.31	18.24	18.50	2.15	6.0826	0.2210	0.2210	0.1170	0.0416	0.0810	0.4810	0.2340	0.00264	0.01167	0.2261	1.588	2.884	0.339	1.200
104*	19.45	16-10	18.47	18.24	18.25	3.20	5.3577	0.2275	0.2340	0.1170	0.1040	0.1231	0.5070	0.2210	0.00048	0.01191	0.0403	1.398	2.540	0.339	-
105	14.90	16-10	18.23	18.07	15.80	1.78	5.5333	0.1820	0.1235	0.0780	0.0364	0.0842	0.7280	0.1950	0.00204	0.00979	0.2079	1.444	2.623	0.254	2.091
106	24.78	16-10	18.86	18.41	20.20	1.95	5.9947	0.2470	0.2535	0.1820	0.0468	0.0875	0.3510	0.3120	0.00352	0.01627	0.2163	1.565	2.842	0.429	1.340
107	34.49	16-10	-	19.00	26.00	2.10	6.4630	0.3380	0.2990	0.2340	0.0416	0.0972	0.3380	0.3250	0.00491	0.02165	0.2269	1.687	3.064	0.610	0.978
108	40.29	16-10	-	19.97	37.63	2.28	6.7145	0.3770	0.3380	0.3380	0.0260	0.0940	0.2990	0.3250	0.00588	0.02449	0.2299	1.753	3.183	0.718	0.839
109*	40.30	16-10	-	20.04	38.44	6.27	5.8806	0.3510	0.3445	0.2080	0.1872	0.1199	0.3380	0.3640	0.00033	0.02213	0.0000	1.535	2.790	0.718	-
110	48.07	16-2	-	18.58	28.96	1.21	7.1465	0.4095	0.3575	0.6630	0.0364	-	0.4680	0.3380	0.00963	0.02957	0.3256	1.885	3.388	0.836	0.730
111	59.52	16-0	-	19.00	36.00	1.39	7.1186	0.4355	0.4290	0.7670	0.0494	-	0.4940	0.3120	0.01171	0.03740	0.3130	1.877	3.375	0.927	0.734
114	37.34	16-0	18.30	17.93	25.39	2.24	6.6163	0.4388	0.3166	-	-	0.1103	0.7774	0.3640	0.00517	0.02284	0.2264	1.734	3.137	-	0.808
115	44.63	15-10	18.44	18.33	30.60	2.12	6.6836	0.4810	0.3705	-	0.0047	0.1168	0.6084	0.3198	0.00689	0.02786	0.2473	1.751	3.169	0.809	0.723
116	50.64	15-10	18.60	18.28	31.27	1.95	6.7826	0.5005	0.3751	-	0.0151	0.1103	0.5759	0.3978	0.00917	0.03183	0.2881	1.777	3.216	0.860	0.558
117	56.32	15-9	18.61	18.48	33.60	1.97	6.7490	0.5265	0.4141	-	0.0411	0.1103	0.5564	0.3848	0.01060	0.03593	0.2950	1.768	3.200	0.956	0.641
118	61.15	15-9	-	20.63	56.50	1.34	6.0013	0.5525	0.4323	-	0.0406	0.1652	0.5044	0.3094	0.01544	0.04863	0.3175	1.566	2.845	1.120	0.588
119	65.05	15-11	-	20.46	55.53	1.65	6.7396	0.5720	0.4553	-	0.0910	0.1069	0.5330	0.4095	0.01289	0.04596	0.2805	1.766	3.195	1.222	0.667
120	69.86	15-10	-	20.32	51.80	1.54	6.2900	0.4553	0.4518	-	0.0614	0.0680	0.4290	0.3640	0.01790	0.05525	0.3240	1.648	2.982	1.323	0.840
122	77.00	16-0	-	20.45	53.36	2.23	6.5910	0.4648	0.4583	-	0.0302	0.0745	0.4420	0.4160	0.01738	0.05634	0.3085	1.727	3.125	1.408	0.784
123	63.70	16-0	-	20.54	54.45	1.36	6.3660	0.5265	0.4225	-	0.0468	0.1069	0.4940	0.3510	0.01300	0.04687	0.2671	1.668	3.018	1.086	0.870
124	74.80	16-0	-	20.80	59.28	1.76	6.6400	0.5590	0.4557	-	0.0572	0.0842	0.5200	0.3640	0.01607	0.04996	0.3216	1.740	3.148	1.289	0.656
125	82.00	16-0	-	20.89	57.64	3.14	6.9830	0.4875	0.4635	-	0.0260	0.0942	0.5070	0.4420	0.01804	0.05002	0.3606	1.830	3.311	1.527	0.579
126	90.10	16-0	-	20.89	58.84	4.91	7.2020	0.4420	0.4635	-	-	0.0972	0.4940	0.4680	0.01947	0.05081	0.3832	1.887	3.414	1.793	0.541
127	60.00	16-0	-	19.95	47.39	3.53	6.9690	0.5005	0.4030	-	0.0364	-	0.5070	0.3510	0.00842	0.03467	0.2429	1.826	3.304	1.015	0.684
128	70.30	16-0	-	20.49	53.88	3.44	6.6500	0.5395	0.4420	-	0.0364	0.0940	0.4680	0.3510	0.01374	0.04400	0.3123	1.742	3.153	1.298	0.661
129	80.00	16-0	-	20.55	54.60	4.08	6.6760	0.5395	0.4680	-	0.0312	0.0842	0.4420	0.3770	0.01647	0.04960	0.3320	1.749	3.165	1.499	0.714
130	90.00	16-0	-	20.65	55.81	5.16	6.6460	0.5395	0.4615	-	-	0.0810	0.3900	0.4160	0.02567	0.05540	0.4633	1.741	3.151	1.838	0.590
131	75.00	15-5	-	20.45	48.38	-	-	-	-	-	-	-	-	-	-	-	-	-	-	-	-
132	69.80	15-5	-	20.15	56.80	-	-	-	-	-	-	-	-	-	-	-	-	-	-	-	-
133	79.80	15-0	-	20.28	63.38	1.51	6.9190	0.5850	0.5140	-	0.1560	0.0778	0.4810	0.4420	0.01778	0.05160	0.3446	1.813	3.280	1.417	0.523
134	77.00	15-3	-	20.02	57.96	0.31	6.8096	0.5980	0.5400	-	0.2704	0.0778	0.7540	0.4160	0.01598	0.04810	0.3322	1.784	3.228	1.247	0.523
135	77.10	15-3	-	20.22	59.59	0.94	6.6415	0.5920	0.5140	-	0.1508	0.0745	0.4550	0.4420	0.02058	0.05307	0.3878	1.740	3.149	1.141	0.526
136	83.20	15-7	-	20.61	60.26	1.32	6.6163	0.5920	0.5140	-	0.1196	0.0616	0.4160	0.4550	0.02270	0.05740	0.3955	1.742	3.137	1.569	0.538
137	87.80	15-7	-	20.18	55.12	2.11	6.6157	0.5920	0.5140	-	0.0396	0.0583	0.4030	0.4810	0.02360	0.05823	0.4053	1.749	3.163	1.714	0.807
138	91.10	15-7	-	20.74	59.48	3.39	6.7424	0.5720	0.5140	-	0.0676	0.0519	0.3900	0.4420	0.02270	0.05840	0.3880	1.762	3.197	1.667	0.535
139	96.00	15-8	-	20.49	57.88	3.42	6.8265	0.5850	0.5100	-	0.0624	0.0486	0.3900	0.5200	0.02435	0.06120	0.3979	1.789	3.236	1.810	0.509
140	96.30	15-8	-	20.18	54.16	3.42	6.9106	0.5720	0.5070	-	0.0520	0.0454	0.4030	0.5460	0.02450	0.05860	0.4181	1.811	3.276	1.864	0.477
141	100.00	15-8	-	20.07	52.88	4.11	6.9106	0.5790	0.5070	-	0.0260	0.0421	0.3510	0.5590	0.02602	0.06120	0.4252	1.811	3.276	1.923	0.473
201	25.10	15-6.5	17.42	16.56	17.38	1.43	6.4593	0.3510	0.2795	-	0.0416	0.1102	-	0.6435	0.00538	0.01579	0.3407	1.694	0.977	0.283	0.497
202	35.00	15-0	17.57	16.68	25.45	0.78	6.4641	0.4420	0.3705	-	0.1456	0.0842	0.9880	0.6110	0.00739	0.02406	0.3071	1.687	3.065	0.571	0.633
203	43.30	15-3	17.51	16.77	34.68	0.39	6.3546	0.4940	0.4420	-	0.3380	0.0810	0.9880	0.7150	0.01086	0.03123	0.3480	1.659	3.013	0.741	0.807
204	43.50	15-6.5	18.20	17.63	28.47	1.50	7.1795	0.4680	0.3868	-	0.0832	0.1102	0.8580	0.3640	0.00781	0.02593	0.3012	1.874	3.044	0.669	0.447
205	51.60	15-7	18.37	17.77	33.28	0.87	7.0532	0.3770	0.4420	-	0.1404	0.1037	0.7670	0.4160	0.01158	0.03280	0.3530	1.841	3.344	0.911	0.667
206	60.20	15-0	18.42	17.91	37.25	0.43	7.0027	0.5395	0.4875	-	0.1976	0.0972	0.7670	0.4550	0.01287	0.03946	0.3261	1.828	3.320	1.038	0.668
207	70.90	14-10	18.55	18.27	42.91	0.0	6.8764	0.5915	0.5395	-	0.2496	0.0713	0.6890	0.4680	0.01706	0.04817	0.3542	1.795	3.260	1.256	0.465
208	35.80	15-10	18.26	17.78	26.28	1.95	7.0027	0.4030	0.3250	-	0.0312	0.1134	0.8580	0.3380	0.00614	0.02079	0.2953	1.828	3.320	0.600	1.298
209	25.60	16-5	18.15	17.89	19.24	2.06	6.7670	0.3250	0.2405	-	-	0.1102	0.8320	0.2340	0.00343	0.01441	0.2880	1.766	3.209	0.396	1.016
210	73.70	16-5.5	-	20.90	53.24	3.50	6.3941	0.5460	0.4485	-	0.0312	0.0812	0.4940	0.3380	0.01761	0.04910	0.3586	1.645	2.990	1.482	1.025
211	76.40	16-5.5	-	20.39	46.45	5.05	6.6071	0.5720	0.4615	-	-	0.0713	0.4940	0.3380	0.01761	0.04603	0.3826	1.724	3.132	1.702	0.946
212	78.90	15-7	-	20.06	53.74	2.58	6.3967	0.5850	0.4875	-	0.0884	0.0583	0.5830	0.4420	0.01773	0.05347	0.3316	1.670	3.033	1.476	0.938

*Lower Feed Ring

$$f^{**} = \left[\frac{V_D R}{V_{ent}} \right] \left[\frac{\sigma}{\sigma_0} \right]^{0.667} \left[\frac{C_D}{C_0} \right] \left[\frac{H(D)}{H(D)-0.5} \right] \left[\frac{H(D)}{H(D)+0.5} \right] \left(\frac{P}{P_0} \right)^{0.5}$$

Table A-2

SUMMARY OF LIQUID CARRYOVER DATA

Power, Mw	Liquid* Carryover	Water Column, ft-in.	Steam Dome, in.	Power, Mw	Liquid* Carryover	Water Column, ft-in.	Steam Dome, in.
53.2	0.0246	15- 3		91.1	0.3049	15- 7	23.52
56.0	0.0377	15- 3		96.0	0.3523	15- 8	24.01
60.7	0.0299	15- 3		96.3	0.3597	15- 8	28.10
61.6	0.0815	14-10		99.1	0.4014	15- 8	29.16
66.8	0.0375	15- 3		99.7	0.3929	15- 8	
67.3	0.0340	15- 3		101.3	0.3765	15- 8	
75.3	0.0679	15- 3	29.04	101.4	0.3785	15- 8	
75.6	0.0064	15- 3		47.0	0.0217	16- 0	
76.6	0.0406	15- 3		59.1	0.0543	15-10	
78.1	0.0104	15- 3		60.0	0.0383	16- 0	
79.8	0.0623	15- 3	27.0	62.7	0.0278	15-10	53.4
84.6	0.1421	15- 3		67.7	0.0529	15-10	
87.3	0.1044	15- 3		68.7	0.0321	15-10	
88.1	0.1138	15- 3		70.1	0.1403	16- 0	24.12
70.3	0.0310	15- 6		73.7	0.2042	16- 2	19.2
71.9	0.0339	15- 5		74.7	0.1913	16- 0	
73.2	0.0149	15- 5		79.5	0.3060	16- 3	
77.1	0.1985	15- 5	27.36	80.3	0.1511	16- 0	23.40
83.2	0.2110	15- 7	23.68	82.0	0.3087	16- 2	21.40
87.8	0.2451	15- 7	24.84	90.9	0.3843	16- 2	22.20

*Weight fraction of liquid in steam.

ARGONNE NATIONAL LAB WEST



3 4444 00008167 9

7